7144 *Macromolecules* **2006,** *39,* 7144−7148

Dynamics of Wormlike Micelles in Elongational Flows

Philip A. Stone,† Steven D. Hudson,*,† Paul Dalhaimer,‡ Dennis E. Discher,‡ Eric J. Amis,† and Kalman B. Migler†

Polymers Division, National Institute of Standards and Technology, Gaithersburg, Maryland 20899, and Chemical and Biomolecular Engineering, University of Pennsylvania, Philadelphia, Pennsylvania 19104

Received May 16, 2006; Revised Manuscript Received August 14, 2006

ABSTRACT: Wormlike micelles provide an opportunity to study the behavior of semiflexible macromolecules in elongational flows. We constructed a microfluidic cross-flow device coupled with fluorescence microscopy to image individual wormlike micelles and measure their dynamics in planar elongational flow. These polymer micelles prove stable in elongational flow and exhibit a sharp transition between regimes where Brownian motion dominates the micellar dynamics and where the micelles stretch with the flow. The coil−stretch transition and micellar relaxation time were identified by examining a distribution of micelle lengths at various flow rates. The relationship between micellar relaxation time and length is consistent with hydrodynamic theory. At higher Weissenberg number, micelle stretching is nearly as rapid as the rate of stretching of the surrounding fluid, yet also results more frequently in sharply folded conformations. In contrast to DNA in extensional flow, these relatively more stiff macromolecules exhibit fewer alignment modes.

1. Introduction

Single molecule studies of DNA have provided much insight into the dynamics of isolated polymers in simple flows.[1−4] In those experiments, a single molecule of genomic-length DNA (several micrometers in length) is labeled with a fluorescent dye and visualized with an optical microscope, while subjected to a simple flow field in a microfluidic device. Such experiments are conducted in viscous solutions (solvent viscosity, $\eta_s \approx 40$ mPa•s) to ensure a steady and sufficiently strong flow. These DNA experiments show that molecules of the same contour length that experience the same strain history can show different stretching dynamics, depending on individual molecular conformation, which are described by the following six classifications: dumbbell, half-dumbbell, kinked, folded, uniform, and coiled.[3]

Stretching DNA in microfluidic devices was originally envisioned as useful for sequencing applications, but scientifically these experiments have allowed for the development and verification of theoretical and computational models. Parameters for bead−spring polymer models[5] have been fit to the experimental DNA data to better understand how hydrodynamic and excluded volume interactions affect the dynamics of polymers in dilute solutions.[6,7] This has allowed studies of the effect of hydrodynamic interactions on the dynamics of polymers in flow geometries where the device dimensions are the same order as the polymer equilibrium radius of gyration.[8]

Given the success of the single molecule experiments with DNA in elongation flow, we seek other rheologically interesting "molecules", which may exhibit different dynamical behavior. Diblock copolymers of appropriate structure form long wormlike micelles that can be visualized and that have applications in understanding the physics of biological structures.[9−11] An advantage of the wormlike micelles in single "molecule" visualizations is their relatively large persistence length compared to the limiting resolution of optical microscopes. The persistence length of the wormlike micelles is 500 ± 200 nm,[12] while the persistence length of fluorescently labeled DNA is less than 100 nm.[13] Unlike DNA, the persistence length of the micelles is within the (classical) limit of minimum resolvable size (i.e., ~$^1/_2$ the wavelength of light used). Using fluorescent micelles, the dynamics on length scales of the same order of the persistence length can be resolved. Macromolecular dynamics at length scale smaller than the persistence length have been observed, for example, in flowing solutions of actin filaments[14] and quiescent solutions of carbon nanotubes.[15]

One major difference of the micellar system, and these others, compared to the DNA experiments is the lack of monodispersity. The wormlike micelles can form with contour lengths that vary from submicrometer to submillimeter scales.[12] The length distribution of the wormlike micelles is also not necessarily fixed with time. Given a high enough tension in a micelle, it can break into two or more pieces, which might, depending on concentration and the subsequent applied stress, unite with other micelles or break into even smaller pieces. However, as described below, we utilize the length distribution to measure the dynamics of numerous length chains simultaneously, and we did not observe tensile breakage of the micelles.

In this paper, we demonstrate that wormlike micelles are another type of macromolecule for which single-chain dynamics in flow fields can be studied. We investigate the coil−stretch transition in elongational flow, the alignment kinetics, and macromolecular conformations.

2. Experimental Section

We study the wormlike micelles in a planar, elongational flow generated in a simple, microfluidic device. The device, which has a cross-channel design, was fabricated using a soft lithography technique, described elsewhere in detail.[16,17] A design for the device is printed on transparency film (CG3300; 3M[18]) using a 1200 dpi laser printer. (The printed design is the inverse of that shown in Figure 1.) An optical adhesive (NOA 81; Norland Products) is poured onto a smooth poly(dimethylsiloxane) (PDMS) surface. A (25 × 75 × 1 mm^3) glass slide (Fisher Scientific) is cleaned in a UVO cleaner (model no. 342; Jelight Co., Inc.) for 30 min. The slide is placed atop the adhesive with the cleaned side down (in contact with the adhesive). Two thicknesses of aluminum foil

---

† National Institute of Standards and Technology.
‡ University of Pennsylvania.

10.1021/ma0611016 CCC: $33.50

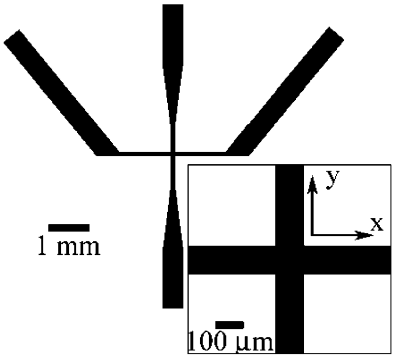

Figure 1. A negative image of the mask used to make the device. The inset shows an enlarged view of the channel junction where the elongational flow is generated.

(Reynolds Heavy Duty) are placed under each end of the glass slide to act as spacers so that adhesive of a depth of about 100 μm remains between the glass slide and the PDMS bottom. The mask is then placed over the glass slide, and the adhesive is exposed to an ultraviolet (UV) light source ($\lambda = 365$ nm) at an intensity of 100 μW/cm^2 for 10 min. This UV radiation dose cures the optical adhesive over the entire depth and binds the adhesive to the glass slide.

After exposure, the glass slide is carefully lifted from the spacers and rinsed with a mixture of acetone and ethanol to remove any uncured adhesive. Once the uncured adhesive is cleaned from the device negative, it is again placed under the UV source to receive a radiation dose of at least 20 times the original dose. This hardens the negative sufficiently to use in making a cast in PDMS. The glass slide with the attached negative side up is placed in a tray made of aluminum foil. The PDMS prepolymer and curing agent (Sylgard 184; Dow Corning) are mixed in a 10:1 mass ratio and degassed. The prepolymer mixture is carefully poured into the tray holding the negative. The tray is placed under vacuum to remove any air bubbles. The PDMS is cured at 75 °C for at least 1 h.

After the PDMS has fully cured, the PDMS is cut with a razor blade to be no larger than the (22×22 mm^2) coverslip to which the device will eventually be sealed. A margin of 3−4 mm is maintained between the arms of the device and the cut in the PDMS. The PDMS device is then carefully peeled away from the glass slide and negative. The cast of the device is temporarily placed on a clean glass slide. The side with the microfluidic device imprint (i.e., the "bottom" side) is in contact with the slide. With a 16 gauge syringe needle, holes are punched through the top of the PDMS to the end of the arms of the device. These holes are used to run tubing to the device. Fine-pointed forceps are used to remove the PDMS plugs from the holes. This is done under a stereo microscope to ensure that all stray fragments of PDMS are removed and not left to clog the device during experiments. After the holes are bored and cleaned, the device is sealed to a no. 1.5 coverslip (22×22 mm^2; Corning Labware and Equipment). The coverslip is cleaned with distilled water and acetone and placed in the UVO cleaner for 30 min. With 1.5 min of cleaning time remaining, the PDMS device is also placed in the UVO cleaner, bottom side up. The coverslip and PDMS cast are removed from the UVO cleaner, and their cleaned surfaces are pressed together firmly. The joined pieces are then placed in a 75 °C oven for at least 2 h to seal the PDMS to the coverslip.

Four pieces of Teflon tubing, 1/32 in. (0.079 cm) i.d., 1/16 in. (0.16 cm) o.d. (EW-06407-41; Cole-Parmer Instrument Co.), are connected to the device. These pieces of tubing are about 5 cm in length. These tubes are carefully pushed as far as possible into the holes previously bored into the PDMS. The tubes are fixed in place using an epoxy (Double/Bubble Epoxy, Extra Fast Setting; Elementis Specialties, Inc.). To help the epoxy adhere to the Teflon, the exterior of each tube is lightly scored with forceps. A bead of epoxy is also placed where the PDMS contacts the coverslip to further ensure a tight seal between these components. After the epoxy has completely hardened, the two outflow tubes, i.e., the tubes connected to the "bent" sidearms of the device as seen in Figure 1, are joined together with a tee fitting to form a single exit line. Having these tubes join together helps to balance the pressure (and, thus, the flow rate) in the two exit arms, providing a more stable elongational flow. A 5 mL plastic syringe is attached to the single exit line to collect the expelled fluid.

The two inlet tubes, which connect to the two vertical arms (Figure 1), are connected to two larger diameter tubes (3.175 mm, Nalgene, 8000-0020). These tubes are joined to a tee that has its single input line connected to a pressure PID controller (ER3000, Tescom Corp.). This pressure controller is supplied with N$_2$ at 310 kPa (45 psig). The pressure drop when using only the microfluidic device filled with water was too small and below the resolution of the PID pressure controller; therefore, a steady flow could not be attained. Two additional measures were taken to increase the pressure drop through the system. First, a 20 cm length of stainless steel capillary tubing with an internal diameter of 0.0039 in. (0.01 cm) was inserted between the pressure regulator and the inlet tee junction. Only nitrogen gas flowed through this tubing. Second, two 1.0 μm syringe filters were added, in series, between the outlet line and the waste-collecting syringe.

To fill the device, the input lines to the microfluidic device are disconnected from the tee that connects to the pressure regulator. The syringe at the end of the output line is disconnected and filled with a solution of 50 wt % glycerin and water. The syringe is reconnected to the output line, and the fluid is injected by hand into the device. Care is taken to ensure that no air bubbles are present in the output lines, input lines, or microfluidic device. The device is filled until two inlet arms are completely filled. A micellar solution of 0.2 mg/mL of diblock copolymer (described below) in a 50 wt % glycerin/water solution is prepared in a 1 mL syringe. The solvent viscosity at the experimental temperature (23 °C) is ~5 mPa·s.[19] Then, ~0.1 mL of the micellar solution is added to one of the input lines. Again, care is taken to avoid introducing air bubbles into the inlet line. Once filled, the input lines are reconnected to the tee that connects to the pressure regulator. Since the flow cannot be stopped within 0.1 s, we did not measure micelle relaxation time directly but estimated it from the observed coil−stretch transition.

The micelles are formed of diblock copolymers consisting of 55 repeat units of poly(ethylene oxide) and 45 repeat units of polybutadiene with a molar mass, $M_n = 4.9$ kg/mol. The block copolymers were produced by an anionic polymerization technique.[20] For this weight fraction of poly(ethylene oxide), $w_{PEO} = 0.51$, the block copolymers form wormlike micelles in aqueous solution with total diameter $d = 29$ nm.[21] A hydrophobic, fluorescent dye (PKH26; Sigma) is added to the aqueous solution at a molar ratio of 1:3 dye/copolymer.[12] The number- and weight-average micelle lengths (L_n and L_w) are approximately 3.5 and 7 μm, respectively. The persistence length of the unstained micelles is reported to be 0.57 μm,[22] and that of stained micelles is 0.5 ± 0.2 μm.[12] Therefore, L_n and L_w respectively comprise approximately 3.5 and 7 statistical Kuhn segments and represent average equilibrium end-to-end distance R_0 of 1.9 and 2.7 μm. The largest micelles observed have $L \approx 25$ μm and $R_0 \approx 5$ μm, dimensions much smaller than the microfluidic channel. The dynamics of these micelles are therefore expected to be equivalent to that in unconfined solutions.[23]

The microfluidic device is mounted on the stage of an Olympus IX71 inverted microscope. The micelles are viewed using an Olympus UPLAPOXW3 water-immersion objective lens, which has 60× magnification, 1.2 NA, and 0.28 mm working distance and is coverslip corrected. Focus was adjusted to the midplane by focusing on the top and bottom surfaces of the channel and splitting the difference. Images of the micelles were captured with a CCD camera (Adimec-1000M) with an exposure time of 38 ms.

Of interest is the maximum projected length R of the micelle (see inset c, Figure 3). The lengths R were corrected for blurring by subtracting the projected distance traveled during exposure from the observed distance R'. The velocity field was measured for each

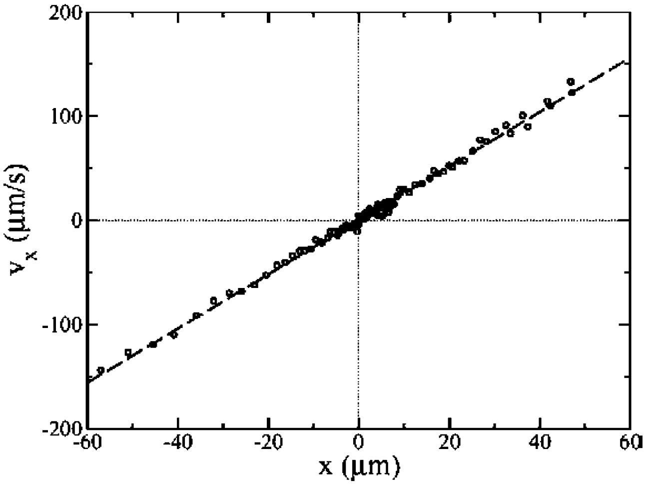

Figure 2. Velocity in the outflow direction of the microfluidic device. The circles are the measured v_x data. The dashed line is a linear regression of the data. The velocity follows that of planar elongational flow, $v_x = \dot{\epsilon}x$, for $\dot{\epsilon} = 2.5\ \mathrm{s}^{-1}$.

image sequence (e.g., see Figure 2). When the signal-to-noise is too small, *R* is underestimated. To maintain sufficient signal-to-noise (here ranging from 5 to 30), only those micelles sufficiently close to the stagnation point that their speed is less than 120 μm/s were measured, so that the blurring in all cases was less than 5 μm. Most of the time during observation the micelle was traveling more slowly, so that blurring was much less. In addition, to ensure sufficient residence time and extensional flow type, only those micelles that enter within 12 μm of the inlet channel centerline are used for measurement. The contour length *L* was measured for those micelles that reach essentially full extension, i.e., $L \approx R$(fully extended).

3. Results and Discussion

The cross-channel device is capable of producing a close approximation to planar elongational flow,

$$\mathbf{v} = \begin{bmatrix} \dot{\epsilon} & 0 & 0 \\ 0 & -\dot{\epsilon} & 0 \\ 0 & 0 & 0 \end{bmatrix} \cdot \mathbf{x} \tag{1}$$

where $\mathbf{v}(x)$ is the fluid velocity at the point $x = (x,y,z)$ and $\dot{\epsilon}$ is the constant elongation rate. With respect to the microfluidic device, the *x*-axis corresponds to the outflow channels and the *y*-axis corresponds to the inflow channels. There is no flow in the *z*-direction. For this flow, the velocity gradient

$$\nabla v = \begin{bmatrix} \dot{\epsilon} & 0 & 0 \\ 0 & -\dot{\epsilon} & 0 \\ 0 & 0 & 0 \end{bmatrix} \tag{2}$$

is not a function of position, so the micelles experience the same velocity gradient at every point in the planar elongational flow. Unlike the model planar elongational flow, the flow in the microfluidic device is confined by upper and lower surfaces (i.e., planes perpendicular to the *z*-axis). Since the fluid at these surfaces is assumed to obey the no-slip boundary condition, a velocity gradient exists in the *z*-direction. To minimize the effect of this velocity gradient, we image the micelles near the midpoint between the upper and lower surface where this velocity gradient is zero.

Figure 2 shows the velocity measured in the device. The velocities were calculated by measuring the change in the *x*-position of the center of mass of a micelle and dividing by the time lapse between the frames. Data from over 10 micelles are plotted in the figure. Most of these micelles are small enough ($L \sim 1$ μm) that they represent a single bead and thus travel as a rigid particle. The velocity is linearly proportional to the distance from $x = 0$ over a range $-60\ \mu\mathrm{m} < x < 60\ \mu\mathrm{m}$, which covers the entire *x*-extent of the camera's field of view and approaches the channel entrances (the corners are somewhat rounded). This calculation was repeated for each data set (a total of ∼40 sets) to determine its extension rate. Several hundred total micelles were tracked and more than 50 with sufficient length for analysis of alignment conformation.

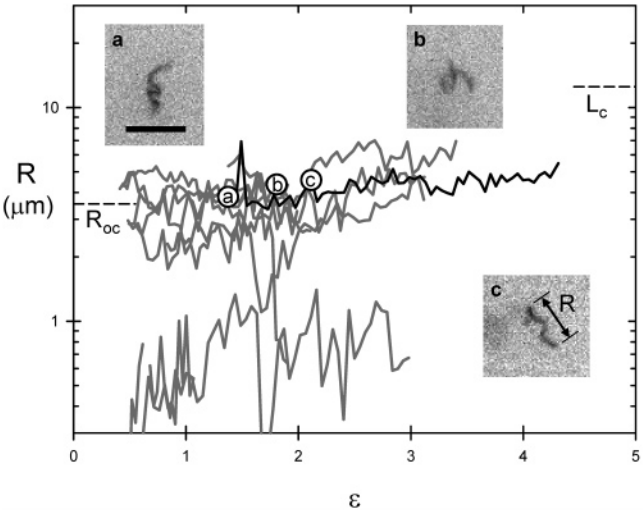

Figure 3. Representative curves (shown gray) for the size R of micelles (see text and inset c) at $\dot{\epsilon} = 0.5\ \mathrm{s}^{-1}$, ranging from somewhat less than 1 to ∼5 μm. The contour length *L* of these larger micelles is nearly 20 μm. The micelles exhibit very little stretch and preferred orientation throughout observation; micellar dynamics are dominated by Brownian motion, indicating that the relaxation time of these longer micelles is no more than ∼1 s (see text). To illustrate the shape of an individual curve, it is shown in black ink. Inset are images of three micelles, whose instantaneous states are plotted with labeled circular symbols. The contrast has been inverted so that the micelles appear dark. The scale bar in inset (a) is 5 μm. On the basis of micelle images, we assume that the distribution of dye along the length of the micelle is nearly uniform and that variations of intensity relate to sharpness of focus, molecular motion, and superposition of multiple segments. The horizontal dashed line at left approximates these coil sizes R_{oc}, and their corresponding extended length L_{c} is indicated by the dashed line at right. Inset c illustrates measurement of R' (which here is essentially equivalent to the projected length of the micelle *R*).

The use of planar elongation allows us to determine how micelles are stretched and oriented in a flow field. Figure 3 shows representative curves of the extension for micelles in a planar elongation with $\dot{\epsilon} = 0.5\ \mathrm{s}^{-1}$. The micellar extension *R* is plotted against the total strain, determined from the product of the extension rate and the residence time. Since the first image of each micelle is already in the extensional flow field, the initial residence time t_0 for each micelle is approximated, consistent with the flow kinematics, as shown in Figure 2

$$t_0 \approx \frac{1}{\dot{\epsilon}} \ln\left(\frac{y_0}{y(t_0)}\right) \tag{3}$$

where $y(t_0)$ is the center of mass of the micelle at time t_0, relative to the line of stretching through the stagnation point, and y_0 is the position at which extensional flow begins. The effective magnitude of y_0 (of order *w*, the width of the channel) is here ∼100 μm.

At this flow rate, Brownian motion dominates, and chains fluctuate in conformation. Only the largest micelles extend, and

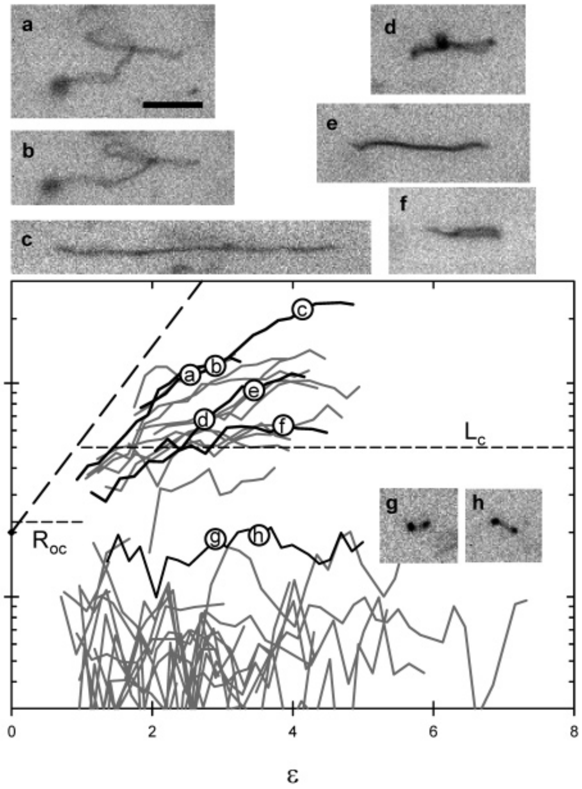

Figure 4. Representative curves for the extension of micelles at $\dot{\epsilon} = 2.5\ \mathrm{s}^{-1}$. Each curve shows the stretch of an individual micelle. Selected curves are shown in black. Stretching of larger micelles by the flow dominates over their Brownian motion. As in Figure 3, the scale bar is 5 μm, and data points corresponding to inset images are labeled. Insets a−c show the same micelle at different points in time. Insets d and e show a micelle whose intermediate conformation is kinked. (f) illustrates a folded micelle, and (g) and (h) show a short micelle that fluctuates in orientation and degree of extension. The bold dashed line indicates the rate of affine stretching, and the finer horizontal dashed lines approximate the micelle length L_c and coil size R_{oc} corresponding to the coil−stretch transition at this flow rate.

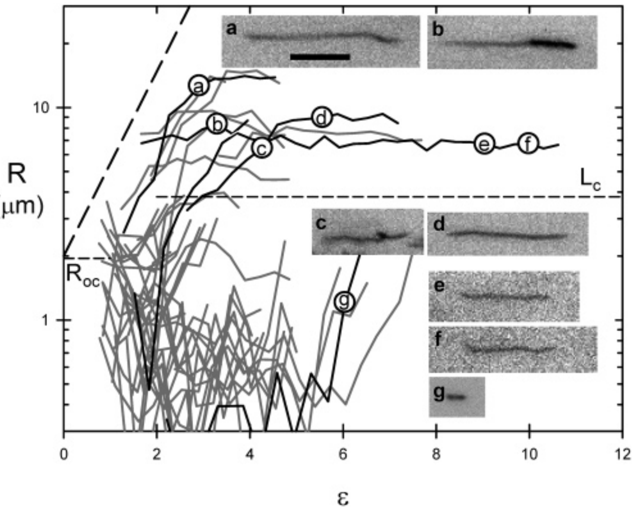

Figure 5. Representative curves for the extension of micelles at $\dot{\epsilon} = 4.0\ \mathrm{s}^{-1}$. Each curve shows the stretch of an individual micelle. Folded and kinked micelles are shown in (b) and (c), respectively. While the former stretches very slowly, the latter extends in due course (d). Weak fluctuations of aligned micelles are shown in (e) and (f). Dashed lines and labels are consistent with the scheme in Figure 4.

these do so only very slowly and weakly, suggesting that the effective Weissenberg number ($\mathrm{Wi} = \dot{\epsilon}\tau$) for those micelles that begin to stretch is near the critical value Wi_c for the coil-to-stretch transition, namely ~0.5. The value of $\mathrm{Wi}_c \cong 0.5$ is robust to changes in chain length ($N \geq 4$) and strength of hydrodynamic interaction.[5,24] The transition broadens somewhat as N approaches unity.[5,25] For a polydisperse sample of chain lengths, sufficiently long micelles may extend, whereas shorter ones do not. We thus identify a critical minimum micelle length L_c for alignment, and we estimate the relaxation time for micelles of this length from the product of Wi_c and the inverse of strain rate, i.e., $\tau(L = L_c) \approx \mathrm{Wi}_c/\dot{\epsilon}$. Since the micelles do not fully extend here, we estimate the coil size of the critical micelle length $R_{oc} \approx 3.5\ \mu$m, $L_c \approx 12-13\ \mu$m, and $\tau(L = 12.5\ \mu\mathrm{m}) \approx 1$ s. A comparable relaxation time was measured in confined quiescent solutions,[12] considering differences in confinement,[23] solvent viscosity, and micelle length.

At $\dot{\epsilon} = 2.5\ \mathrm{s}^{-1}$, substantially more stretching of micelles is observed (Figure 4). For those whose length is greater than $L_c \approx 5\ \mu$m, near complete alignment is observed (e.g., insets c and e), whereas shorter ones exhibit random fluctuations in orientation and extension (e.g., insets g and h). As before, we recognize this as the coil-to-stretch transition, so that $\tau(L = 5\ \mu\mathrm{m}) \approx 0.2$ s.

When aligned, the micelles are not completely straight, but they wiggle and flap, with R nearly equal to L. L is estimated from the length of these aligned conformations. Other aligned micelles are folded (e.g., inset f); some remain so, and others eventually unfold. The onset and rate of micelle stretching are variable, depending on individual micelles and their conformation. Once stretching begins, the rate of stretching of most micelles is considerably slower than that of the surrounding fluid (compare data with the affine stretching curve, Figure 4). We assume that a sufficient number of micelles are observed for sufficiently long that the critical micelle length can be approximated effectively.

Even the longest micelles here have relatively few Kuhn steps. It is therefore difficult to group the conformations among those classes previously identified (dumbbell, folded, coiled, etc.).[3] A more appropriate classification for chains with fewer segments was discussed by Larson et al.[26] This classification was based on simulated initial random conformations, as to whether or not they were prone to fold and concerning the initial random orientation of the chain relative to the stretching axis. While the orientation has some effect on alignment kinetics, those conformations that are fold-prone exhibit more dramatic differences in stretching kinetics. In our experiments, observations begin at finite strain, so that the initial conformation is inaccessible. Therefore, here we classify micelles (those with L greater than the coil−stretch transition) simply whether they attain essentially complete alignment or remain folded or kinked during the time of observation. At $\dot{\epsilon} = 2.5\ \mathrm{s}^{-1}$, roughly 70−80% reach essentially complete alignment.

At still higher rates, $\dot{\epsilon} = 4\ \mathrm{s}^{-1}$, more micelles align, and they do so more rapidly (Figure 5). The coil−stretch transition occurs now at approximately $L_c = 3.8\ \mu$m, so that $\tau(L = 3.8\ \mu\mathrm{m}) \approx 0.125$ s. Micelles longer than L_c align, and shorter ones do not.

The longest micellar relaxation time is predicted to be

$$\tau = \frac{\zeta b^2}{6kT}\tilde{a}_1^{\ -1} = \frac{\pi b^3 \eta}{2kT\ln(b/d)}\tilde{a}_1^{\ -1}$$

where b is the length of the Kuhn segment, ζ is the friction coefficient (which is here expressed for rodlike segments), η is the solvent viscosity, and $\tilde{a}_1$ is the first nonzero eigenvalue of the modified Rouse matrix.[5,27] This eigenvalue describes the effect of micelle length as well as interactions such as hydrodynamic interaction among segments. The hydrodynamic interaction parameter[28] h^* is modest in this case, i.e., $h^* = \sqrt{3/\pi}/(2\ \ln(b/d)) \approx 0.14$, so that (for intermediate N) τ scales approximately as ($N^{1.7}$).[5,29] Although this scaling is consistent with the data—i.e., τ, L pairs: (0.125 s, 3.8 μm), (0.2 s, 5 μm), and (1 s, 12.5 μm)—the predicted relaxation time is ~6 times larger that these experimental estimates. Similarly long relaxation times are predicted by a theory for semiflexible rods.[30] Although agreement with the data could be achieved by reducing either b or η, this discrepancy remains unexplained.

The micelles experience some flow history passing first through a taper and then a channel of constant cross section before entering the cross slot. Does this history influence their initial conformations? Finite element calculations indicate that the center line velocity accelerates by a factor of 6.1 upon passing through the taper (a 5:1 contraction), and a fluid element on the center line experiences a stretching strain of $\ln(6.1) = 1.8$. At the fastest flow rate, the residence time in the taper is ~20 s. The average strain rate is therefore quite weak, less than 0.1 s^{-1}. The elongational rate in the taper is considerably nonuniform, however, and reaches an instantaneous maximum of ~0.5 s^{-1}. The amount of strain applied at a rate greater than 0.25 s^{-1} is merely 0.5 unit. Therefore, at this highest flow rate, the elongational rate is marginal for the largest micelles, and subcritical for most, and the residence time in the taper is short enough that little deformation is induced (compare Figure 3 at a strain of 0.5). This deformation may relax as the chain passes through the inlet channel of constant cross section, and the residence time is inversely proportional to the flow rate. At the fastest flow rate, the residence time at this quasi-quiescent condition is ~2 s. Therefore, at this highest flow rate we expect preconditioning to be insufficient to cause appreciable deformation. It may, however, influence the distribution of initial conformations.

During observation in the cross slot, there remains a distribution of micellar stretching rates (Figure 5), but especially the larger micelles, i.e., those having a larger Wi number, extend with a rate that is nearly affine. Some micelles remain unextended for a few strain units before they finally stretch. A greater fraction of stretched micelles are incompletely stretched, and a fold or kink remains. In this case, only 50−70% reach essentially complete alignment. Similarly, the formation and survival of folds and kinks were also observed in simulations[26] and DNA experiments[3] to be more prevalent at higher Wi.

4. Conclusions

Wormlike micelles, as well as having many commercial applications, make interesting models for semiflexible polymers and biological structures. We studied the dynamics of wormlike micelles in planar elongational flow by means of single micelle visualization using fluorescence microscopy. The coil−stretch transition was identified experimentally, using a distribution of micelle lengths and different flow rates. This transition is sharp, causing distinct populations of stretched and unstretched micelles to appear (Figures 4 and 5).

Stretching rates of a micelle depend on its conformation. Generally, faster rate of alignment and more affine deformation were observed at higher Wi number. Nevertheless, these conditions also resulted in more frequent folded conformations.

References and Notes

(1) Larson, R. G.; Perkins, T. T.; Smith, D. E.; Chu, S. In *Flexible Polymer Chain Dynamics in Elongational Flow: Theory and Experiment;* Nguyen, T. Q., Kausch, H.-H., Eds.; Springer: New York, 1999.
(2) Perkins, T. T.; Smith, D. E.; Chu, S. *Science* **1997**, *276*, 2016.
(3) Perkins, T. T.; Smith, D. E.; Chu, S. In *Flexible Polymer Chain Dynamics in Elongational Flow: Theory and Experiment*; Nguyen, T. Q., Kausch, H.-H., Eds.; Springer: New York, 1999.
(4) Smith, D. E.; Babcock, H. P.; Chu, S. *Science* **1999**, *283*, 1724.
(5) Bird, R. B.; Curtiss, C. F.; Armstrong, R. C.; Hassager, O. *Dynamics of Polymeric Liquids;* Wiley: New York, 1987; Vol. 2.
(6) Jendrejack, R. M.; de Pablo, J. J.; Graham, M. D. *J. Chem. Phys.* **2002**, *116*, 7752.
(7) Schroeder, C. M.; Shaqfeh, E. S. G.; Chu, S. *Macromolecules* **2004**, *37*, 9242.
(8) Jendrejack, R. M.; Schwartz, D. C.; de Pablo, J. J.; Graham, M. D. *J. Chem. Phys.* **2004**, *120*, 2513.
(9) Dalhaimer, P.; Bermudez, H.; Discher, D. E. *J. Polym. Sci., Part B: Polym. Phys.* **2004**, *42*, 168.
(10) Discher, B. M.; Won, Y. Y.; Ege, D. S.; Lee, J. C. M.; Bates, F. S.; Discher, D. E.; Hammer, D. A. *Science* **1999**, *284*, 1143.
(11) Jain, S.; Bates, F. S. *Science* **2003**, *300*, 460.
(12) Dalhaimer, P.; Bates, F. S.; Discher, D. E. *Macromolecules* **2003**, *36*, 6873.
(13) Shaqfeh, E. S. G. *J. Non-Newtonian Fluid Mech.* **2005**, *130*, 1.
(14) Koster, S.; Steinhauser, D.; Pfohl, T. *J. Phys.: Condens. Matter* **2005**, *17*, S4091.
(15) Duggal, R.; Pasquali, M. *Phys. Rev. Lett.* **2006**, *96*, 246104.
(16) Harrison, C.; Cabral, J.; Stafford, C. M.; Karim, A.; Amis, E. J. *J. Micromech. Microeng.* **2004**, *14*, 153.
(17) Cabral, J. T.; Hudson, S. D.; Harrison, C.; Douglas, J. F. *Langmuir* **2004**, *20*, 10020.
(18) Certain commercial materials and equipment are identified in this paper in order to adequately specify the experimental procedure. In no case does such identification imply recommendation or endorsement by the National Institute of Standards and Technology, nor does it imply that these are necessarily the best available for the purpose.
(19) Dow Chemical, Viscosity of aqueous glycerine solutions. http://www.dow.com/glycerine/resources/viscosity.htm 2006.
(20) Hillmyer, M. A.; Bates, F. S. *Macromolecules* **1996**, *29*, 6994.
(21) Won, Y. Y.; Paso, K.; Davis, H. T.; Bates, F. S. *J. Phys. Chem. B* **2001**, *105*, 8302.
(22) Won, Y. Y.; Davis, H. T.; Bates, F. S.; Agamalian, M.; Wignall, G. D. *J. Phys. Chem. B* **2000**, *104*, 7134.
(23) Jendrejack, R. M.; Dimalanta, E. T.; Schwartz, D. C.; Graham, M. D.; de Pablo, J. J. *Phys. Rev. Lett.* **2003**, *91*, 038102.
(24) Cifre, J. G. H.; de la Torre, J. G. *J. Rheol.* **1999**, *43*, 339.
(25) Liu, S.; Ashok, B.; Muthukumar, M. *Polymer* **2004**, *45*, 1383.
(26) Larson, R. G.; Hu, H.; Smith, D. E.; Chu, S. *J. Rheol.* **1999**, *43*, 267.
(27) Zimm, B. H. *J. Chem. Phys.* **1956**, *24*, 269.
(28) Thurston, G. B.; Peterlin, A. *J. Chem. Phys.* **1967**, *46*, 4881.
(29) Thurston, G. B. *Polymer* **1974**, *15*, 569.
(30) Pasquali, M.; Shankar, V.; Morse, D. C. *Phys. Rev. E* **2001**, *6402*, 246104; for corrected coefficients, see ref 15.

MA0611016